Synthetic matrices reveal contributions of ECM biophysical and biochemical properties to epithelial morphogenesis

Nduka O. Enemchukwu,[1,2] Ricardo Cruz-Acuña,[2,3] Tom Bongiorno,[1,2] Christopher T. Johnson,[2,3] José R. García,[1,2] Todd Sulchek,[1,2] and Andrés J. García[1,2]

[1]Woodruff School of Mechanical Engineering, [2]Petit Institute for Bioengineering and Bioscience, and [3]Coulter Department of Biomedical Engineering, Georgia Institute of Technology, Atlanta, GA 30332

Epithelial cells cultured within collagen and laminin gels proliferate to form hollow and polarized spherical structures, recapitulating the formation of a rudimentary epithelial organ. However, the contributions of extracellular matrix (ECM) biochemical and biophysical properties to morphogenesis are poorly understood because of uncontrolled presentation of multiple adhesive ligands, limited control over mechanical properties, and lot-to-lot compositional variability in these natural ECMs. We engineered synthetic ECM-mimetic hydrogels with independent control over adhesive ligand density, mechanical properties, and proteolytic degradation to study the impact of ECM properties on epithelial morphogenesis. Normal cyst growth, polarization, and lumen formation were restricted to a narrow range of ECM elasticity, whereas abnormal morphogenesis was observed at lower and higher elastic moduli. Adhesive ligand density dramatically regulated apicobasal polarity and lumenogenesis independently of cell proliferation. Finally, a threshold level of ECM protease degradability was required for apicobasal polarity and lumen formation. This synthetic ECM technology provides new insights into how cells transduce ECM properties into complex morphogenetic behaviors.

Introduction

Cell–ECM adhesion transduces mechanical and biochemical signals that regulate epithelial morphogenesis (Klinowska et al., 1999; Lubarsky and Krasnow, 2003; Wozniak et al., 2003; Paszek et al., 2005; Yu et al., 2005; Nelson et al., 2006; Bryant and Mostov, 2008; Zhang et al., 2009, 2011). Bissell, Mostov, and others have pioneered the use of 3D collagen and laminin (i.e., Matrigel) gels in organotypic cultures that recreate the epithelial morphogenetic developmental program (O'Brien et al., 2002; Mroue and Bissell, 2013). In these natural matrices, epithelial cells, such as MDCK cells, proliferate from single cells to form multicellular, hollow spherical monolayer structures (cysts) within 10 d that bear the hallmarks of epithelial polarity, recapitulating the morphogenetic program for the formation of a rudimentary epithelial organ (McAteer et al., 1986). These 3D cultures have revealed that interactions between integrin adhesion receptors and secreted laminin and the density of ECM, which impacts the gel mechanical properties, regulate the establishment of cell polarity and morphogenesis as well as tumorigenesis (Barcellos-Hoff et al., 1989; O'Brien et al., 2001; Wozniak et al., 2003; Levental et al., 2009; Provenzano et al., 2009). Nevertheless, these natural matrices are inherently limited by the inability to decouple mechanical properties from matrix and ligand density and lot-to-lot compositional and structural variability (Yu et al., 2005; Hughes et al., 2010). Additionally, tumor-derived matrices such as Matrigel have limited clinical translational potential in regenerative medicine applications. In the work presented here, we describe a modular, synthetic ECM-mimetic hydrogel platform with controlled presentation of cell-adhesive ligands, tunable mechanical properties, and protease-dependent degradation to direct epithelial morphogenesis. Whereas previous work has established synthetic polymer hydrogels as engineered ECMs to investigate single cell behaviors (Lutolf et al., 2003; Kloxin et al., 2009; Huebsch et al., 2010; Khetan et al., 2013) and multicellular assemblies of cancer cell lines with a focus on tumorigenesis (Gill et al., 2012; Weiss et al., 2012; Beck et al., 2013; Raza et al., 2013), we analyze the contributions of ECM mechanical and biochemical properties to the coordinated multicellular epithelial morphogenesis developmental program. Understanding how cells transduce ECM properties into complex morphogenetic behaviors is paramount to developmental biology, pathogenesis, and materials-based regenerative medicine. Finally,

---

The Rockefeller University Press $30.00
J. Cell Biol. Vol. 212 No. 1   113–124
www.jcb.org/cgi/doi/10.1083/jcb.201506055

JCB   113

this platform technology is straightforward to implement and uses commercially available reagents, allowing for facile and broad adoption by the community.

Results

Synthetic PEG hydrogels as ECM mimics with tunable biophysical and biochemical properties

To overcome the inability to tune the mechanical, structural, and biochemical characteristics and lot-to-lot compositional variability of natural ECMs, we engineered synthetic ECM-mimetic hydrogels with independent control over the presentation of cell-adhesive ligand type/density, mechanical and structural properties, and protease-dependent degradation to study the impact of ECM biophysical and biochemical properties on epithelial morphogenesis. These polyethylene glycol (PEG) hydrogels are based on a four-arm PEG macromer with maleimide groups at each terminus (PEG-4MAL; Fig. 1 A). The PEG-4MAL platform outperforms other synthetic chemistries in generating structurally defined hydrogels with stoichiometric incorporation of ligands and improved cross-linking efficiency (Phelps et al., 2012), providing an ideal material platform for the systematic and rigorous evaluation of the effects of ECM biochemical and biophysical properties on cell functions. Furthermore, these hydrogels exhibit superior in vitro and in vivo biocompatibility for several cell types including mesenchymal stem cells, skeletal myoblasts, and pancreatic islets (Phelps et al., 2012, 2013; Salimath et al., 2012). In a rapid reaction with quantitative yields, thiol-containing ligands such as cysteine-containing peptides can be conjugated to the PEG-4MAL macromer via reaction with the maleimide group to yield a functionalized macromer (Fig. 1 A). In this fashion, PEG-4MAL macromers presenting GRGDSPC (RGD) peptide that binds to integrin adhesion receptors were prepared (Fig. 1 A). RGD peptides were tethered onto the PEG-4MAL macromer with high yield (Fig. 1 B), demonstrating precise control over adhesive ligand density. Cysteine-flanked, protease-degradable peptide was then reacted with RGD-functionalized PEG-4MAL macromers in the presence of cells to cross-link macromers into a hydrogel network encapsulating the cells (Fig. 1 A). Importantly, in this synthetic platform, macromer size, polymer density, adhesive ligand type and density, and cross-linker type and density can be independently controlled to tune hydrogel structure (mesh size), mechanical properties, ECM ligand presentation, and protease-dependent degradation. For example, for a given macromer size (e.g., 20 kD PEG-4MAL), hydrogel elastic modulus increases, whereas equilibrium swelling (which is related to hydrogel structure) decreases as a function of polymer density as a tighter network is formed (Fig. 1 C), in excellent agreement with Flory-Rehner theory (Flory and Rehner, 1943; Canal and Peppas, 1989).

A major limitation for natural matrices such as collagen gels and Matrigel is that changes in protein concentration to vary mechanical properties invariably alter adhesive site local density and organization through changes to fiber structure and density. In contrast, for this modular synthetic system, mechanics, degradation, and adhesive ligand presentation can be independently tuned (Fig. 1 D). Because the PEG-4MAL macromers are symmetric and, when cross-linked into a hydrogel, form a regular mesh structure that is fully swollen, the adhesive peptide

is uniformly distributed throughout the hydrogel network within the "statistical mean" of the mesh size. For the 20-kD macromer hydrogel system described here, the mesh size is 30–40 nm. Because of the small size of the PEG macromer arms and the swollen state of the gel, the mobility of the adhesive peptide is very limited. FRAP experiments with fluorescently labeled RGD peptide within hydrogels showed negligible fluorescence recovery, indicating very limited mobility of the adhesive peptide and uniform distribution throughout the hydrogel (Fig. S1 A). We also examined whether the spatial distribution of RGD peptide changes at the cell–hydrogel interface because of cell contractility. Using hydrogels presenting labeled RGD peptide and confocal microscopy, we monitored signal intensity at the cell–hydrogel interface as a function of time for cell cysts (Fig. S1 B). We observed no differences in signal intensity over time for either Y-27632–treated (10 µM) or control cysts, indicating no changes in local ligand density (i.e., clustering) with cell contractility. Taken together, these results demonstrate uniform spatial presentation of the adhesive peptide in a length scale relevant to the cell. Using this modular and well-controlled hydrogel platform, we analyzed the effects of ECM biochemical and biophysical properties on epithelial morphogenesis.

Normal epithelial morphogenesis requires an optimal range of ECM elasticity

We first investigated the influence of hydrogel polymer density, which is analogous to ECM concentration, on epithelial morphogenesis. Single MDCK cells were embedded in PEG-4MAL hydrogels formulated over a range of polymer densities (3.5%–5.0%, wt/vol). This range of polymer densities results in hydrogels with varying mechanical properties (0.85–8.0 kPa elastic modulus) and swelling behavior (Fig. 1 C). All these hydrogels were engineered to present the same density of RGD peptide (2,000 µM) and cross-linked by a fast-degrading, collagen-derived peptide (GPQ-W). This RGD density was chosen based on pilot experiments demonstrating cell attachment and robust spreading on top of such gels (unpublished data). Type I collagen gels (2.0 mg/ml) were used as a reference, because this natural ECM supports epithelial morphogenesis. Single cells embedded in hydrogels formulated at 3.5%, 4.0%, and 4.5% PEG-4MAL remained rounded and maintained high viability at 24 h and, after 48 h, formed multicellular clusters (Fig. 2, A and B; and Fig. S2 A). Formation of these cell clusters did not result from individual cells migrating toward each other, and 5-ethynyl-2′-deoxyuridine (EdU) incorporation confirmed that clusters arose from robust cell proliferation (Fig. 2, A and C). In contrast, cells encapsulated in 5.0% and higher-density PEG-4MAL gels had high viability at 24 h but remained as single and rounded cells at 48 h, with dramatically diminished viability and a complete abrogation of proliferation and formation of multicellular clusters (Fig. 2, A and C). These results demonstrate polymer density–dependent effects on epithelial cell survival and proliferation within PEG-4MAL hydrogels with a nonpermissive barrier at polymer densities of 5.0% and higher.

Columnar epithelia are characterized by polarized distribution of membrane complexes and morphological features between an apical domain facing a lumen/free space and a continuous basolateral domain interfacing with ECM and neighboring cells. This apicobasal polarity is critical for transport, secretion, and barrier functions in several organ systems (Roignot et al., 2013). Furthermore, in morphogenesis of 3D epithelial tissues such as ducts and sacs, establishment of a central
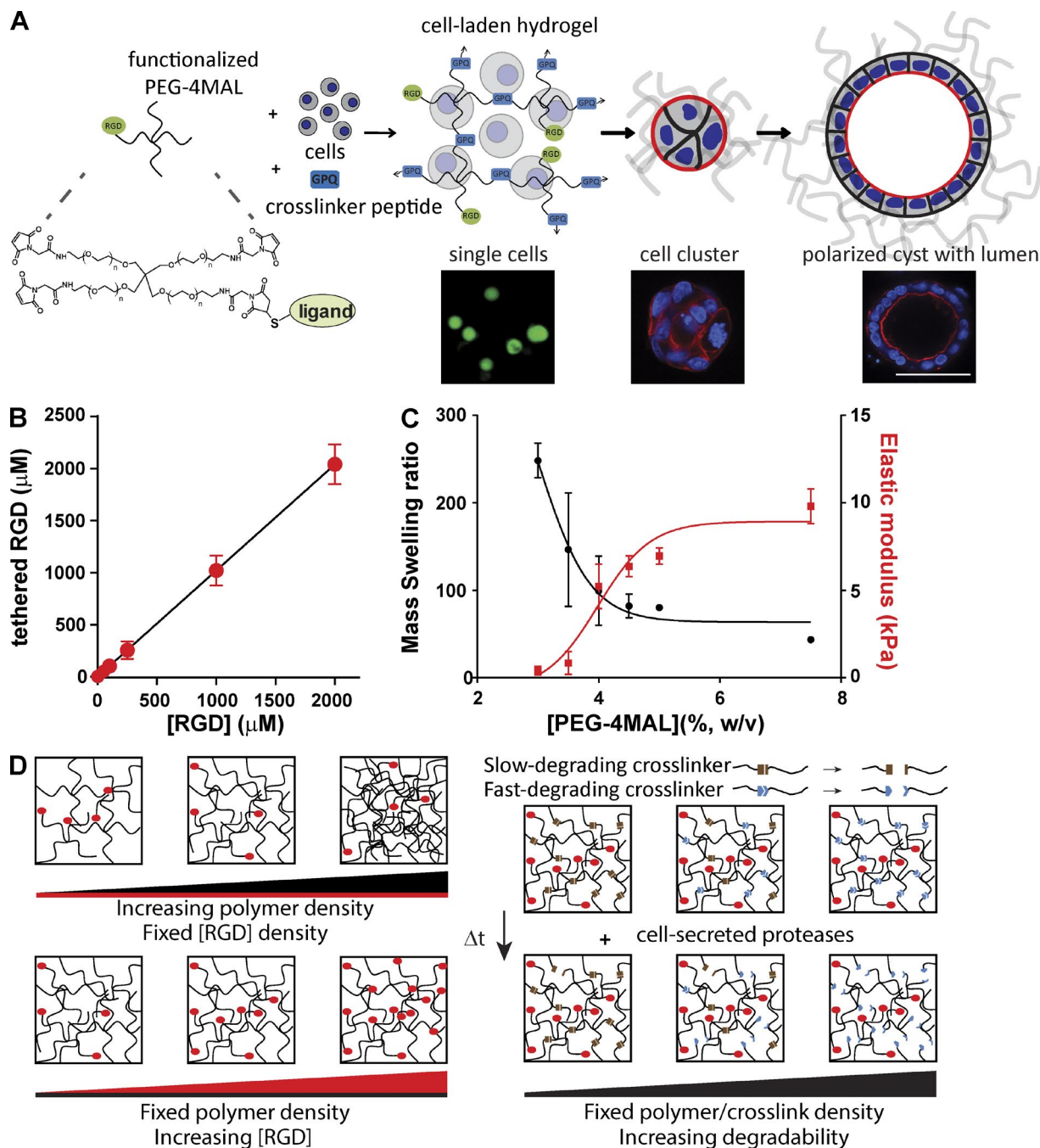
Figure 1. **Synthetic ECMs with tunable biophysical and biochemical properties.** (A) Schematic of cell-encapsulating hydrogel. Adhesive ligand-functionalized 4-arm PEG (PEG-4MAL) is reacted with a thiol-flanked protease-degradable peptide in the presence of cells to form a hydrogel network. Hydrogels support epithelial morphogenesis program. Bar, 50 µm. (B) Tethered RGD density (mean ± SEM) in hydrogel as a function of input RGD concentration. Linear regression: $y = 1.02x + 0.55$, P < 0.0001. (C) Relationship between polymer density (wt%) and hydrogel equilibrium mass swelling ratio (Q_m; left axis, mean ± SEM) and elastic modulus (right axis, mean ± SEM). (D) Cartoon illustrating independent control of polymer density, adhesive ligand density, and cross-link density/network degradation rate in PEG-4MAL hydrogels.

lumen is a critical phase in sculpting tissue architecture (Bryant and Mostov, 2008). For cell proliferation–permissive hydrogel polymer densities, hollowing of the multicellular clusters was visible after 4 d in culture (Fig. S2, A and B). Cleaved caspase-3 labeling indicated the presence of apoptotic cells in developing cysts (Fig. 3, A and B), demonstrating a mode of lumen clearance in permissive hydrogels similar to that observed in collagen gels (Martín-Belmonte et al., 2008). Moreover, MDCK cells in permissive PEG-4MAL hydrogels formed differentiated

epithelial cysts after 10 d in culture consisting of spherical (50- to 100-µm diameter, Fig. 3 C) cellular assemblies with lumens and apicobasal polarity (Fig. 2 D). These well-defined spherical cell structures exhibited canonical markers of apicobasal polarity, including podocalyxin/gp135, actin, ZO-1, GM130, and β-catenin (O'Brien et al., 2006; Fig. S3 A). Cysts in different hydrogel formulations were analyzed for apicobasal polarity and lumen formation using a scoring system (Fig. S3 B). Remarkably, hydrogel polymer density modulated apicobasal
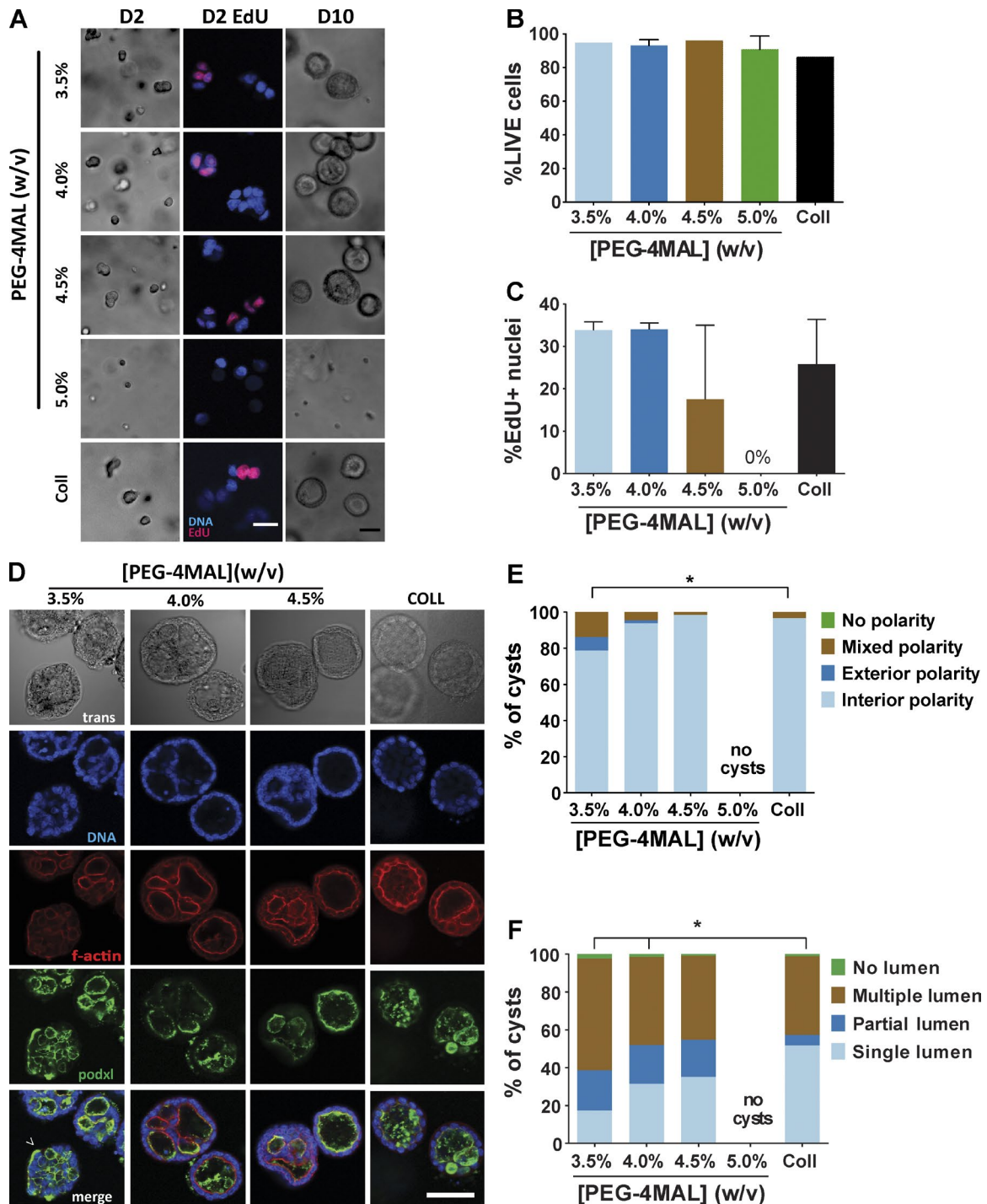
Figure 2. **PEG-4MAL polymer density regulates epithelial morphogenesis.** (A) Transmitted light and fluorescence microscopy images of single MDCK cells cultured in PEG-4MAL hydrogels of different polymer weight percentages over 10 d. At day 2, newly synthesized DNA was labeled by EdU incorporation. Bar, 50 µm. (B) Cell viability (mean ± range in two independent experiments) assessed by calcein-AM (live) and TOTO-3 iodide (dead) labeling at day 1 (>500 cells counted per condition). (C) Proliferation (mean ± range in two independent experiments) as determined by EdU labeling (>590 nuclei counted per condition). (D) Transmitted light and fluorescence microscopy images for MDCK cultures at day 10 and labeled for apical polarity marker gp135/podocalyxin (podxl) and filamentous actin. No cysts were detected in 5.0% PEG-4MAL gels. Bar, 50 µm. (E) Distribution of apical polarity phenotypes at day 10 (>90 cysts analyzed per condition). χ^2 test with Bonferroni's correction; *, $P < 0.014$, 3.5% versus collagen. (F) Distribution of lumen phenotypes at day 10 (>90 cysts scored per condition). χ^2 test with Bonferroni's correction; *, $P < 3 \times 10^{-6}$, 3.5% versus collage; $P < 0.02$, 4.0% versus collagen.

polarity (Fig. 2 E) and lumen formation (Fig. 2 F). Epithelial cysts grown in 4.0% and 4.5% PEG-4MAL gels exhibited normal, internal apical polarity and partial or fully formed single lumens. The frequencies of internal apical polarity and single lumen formation in 4.0% and 4.5% PEG-4MAL gels were equivalent to those for cysts formed in collagen gels (Fig. 2 D–F). In contrast, epithelial cysts grown in 3.5% PEG-4MAL gels exhibited aberrant polarity, with >20% of the cysts
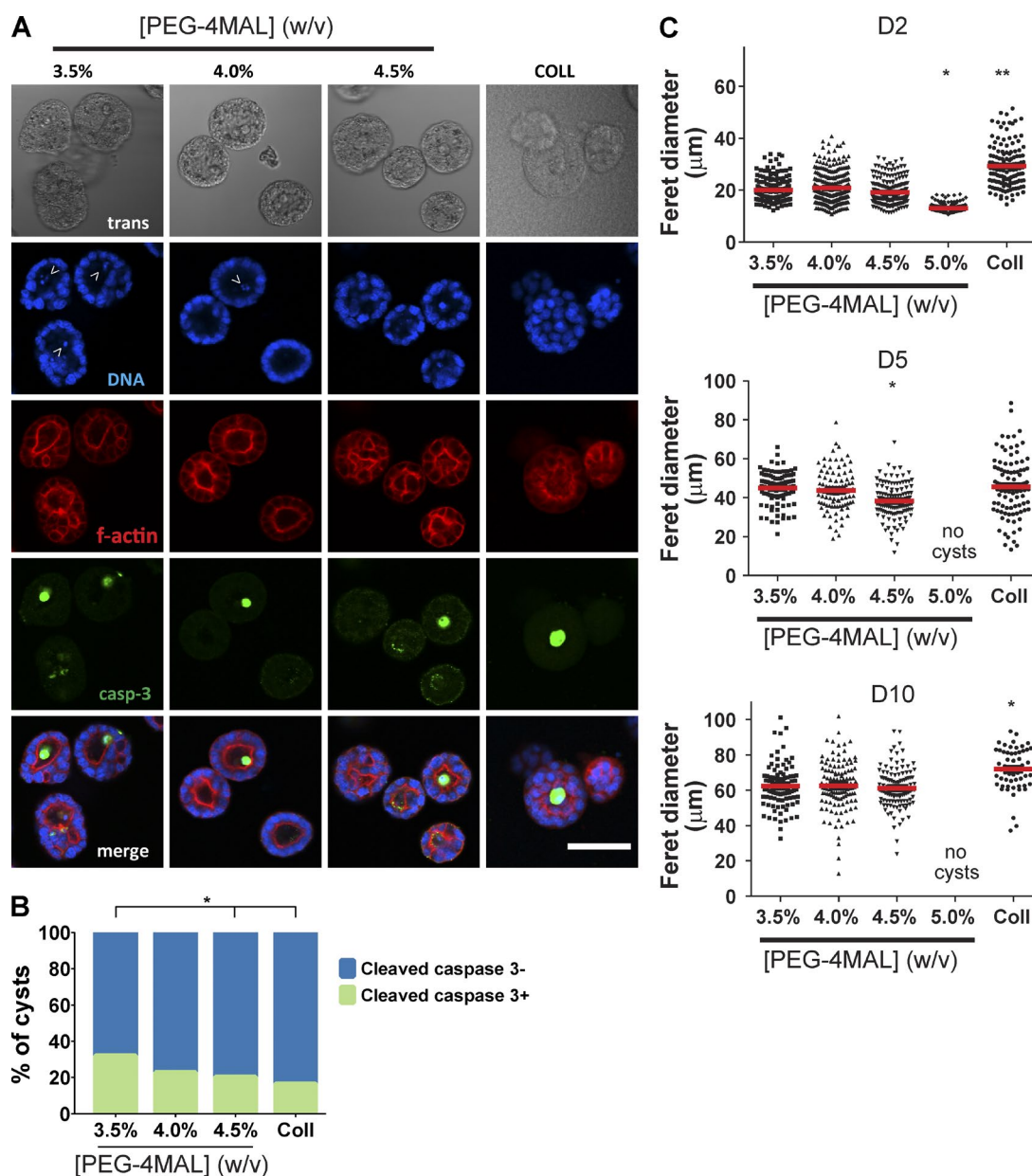
Figure 3. Lumen formation for epithelial cysts within PEG-4MAL hydrogels involves cell apoptosis. (A) Transmitted light and fluorescence microscopy images of MDCK cells cultured within PEG-4MAL hydrogels. Samples were stained for filamentous actin and caspase-3. (B) Distribution of cysts staining positive for caspase-3 (>103 cysts analyzed per condition). χ^2 test with Bonferroni's correction *, P < 0.005, 3.5% versus 4.5% and collagen. (C) Epithelial cyst size (median shown as red line) as a function of PEG-4MAL hydrogel polymer density (>62 cysts analyzed per condition). χ^2 test with Bonferroni's correction. Day 2: *, P < 0.05, 5.0% versus all other polymer densities; **, P < 0.01, 5.0% versus collagen. Day 5: *, P < 0.05, 4.5% versus collagen. Day 10: *, P < 0.05, collagen versus PEG-4MAL groups.

exhibiting mixed or exclusively external (or inverted) polarity (Fig. 2, D and E). Furthermore, only 17% of cysts grown in 3.5% PEG-4MAL exhibited a well-defined single lumen versus 31% and 35% for 4.0% and 4.5% PEG-4MAL gels, respectively (Fig. 2, D and F). Although polymer density regulated polarization and lumen formation, there were no differences in cyst diameter among these permissive hydrogel formulations (Fig. 3 C). No epithelial cysts formed in PEG-4MAL hydrogels with polymer densities of 5.0% and higher.

Normal cyst development, polarization and lumen formation were restricted to a narrow range of hydrogel polymer density, whereas abnormal epithelial morphogenesis and complete abrogation of this developmental program were observed at lower and higher polymer densities, respectively. Because polymer density strongly dictates the mechanical properties of the hydrogel (Fig. 1 C), these results suggest that normal epithelial morphogenesis requires an optimal range of ECM elasticity (E, ~4 kPa). This conclusion is consistent with previous studies reporting changes in epithelial morphogenesis with collagen concentration (Wozniak et al., 2003; Paszek et al., 2005). However, polymer density (as well as collagen concentration) also controls hydrogel structure, as evidenced by changes in swelling behavior (Fig. 1 C), which impacts other important hydrogel properties such as permeability that can influence cell behaviors (Ghajar et al., 2008). To assess whether the polymer density–dependent effects on epithelial morphogenesis were

caused by changes in hydrogel elasticity, we compared cyst polarization and lumen formation in RGD-functionalized hydrogels generated from different macromer sizes (20 vs. 40 kD) but different polymer densities (4.0% vs. 8.0%) engineered to have equivalent mean cross-link densities. Measurements for diffusion of labeled protein (α-bungarotoxin, 8 kD) through these hydrogels demonstrated differences in permeability caused by the differences in macromer arm length (Fig. S4 A). Nevertheless, as expected for gels with equivalent mean cross-link densities, these two gel formulations had equivalent mechanical properties (Fig. S4 B). MDCK cell cyst development proceeded normally in both hydrogel formulations, and there were no differences in polarization or lumen formation between these two formulations (Fig. S4, C and D). This result demonstrates that the effects of polymer density on epithelial morphogenesis are related to hydrogel mechanical properties. Taken together, these results show that normal epithelial morphogenesis requires an optimal range of ECM elasticity.

Adhesive ligand density regulates polarization and lumen formation independently of cell proliferation

We next examined the effects of RGD adhesive ligand density on epithelial morphogenesis within synthetic ECM hydrogels. A constant total density (2,000 µM) of a mixture of cell-adhesive RGD peptide and scrambled inactive RDG peptide was used to vary RGD density (0–2,000 µM) while maintaining identical structures among hydrogel formulations of 4.0% polymer density and constant GPQ-W cross-linking peptide density. Cell proliferation and assembly into multicellular structures was insensitive to RGD peptide density (Fig. 4, A and B). However, epithelial cyst polarity and lumen phenotypes showed a dramatic dependence on RGD density (Fig. 4 C). Hydrogels presenting low (≤100 µM) RGD densities supported the formation of very few cysts with internal apical polarity (<14%), in striking contrast to hydrogels presenting high (≥250 µM) RGD density in which >60% of cysts had internal apical polarity (Fig. 4, C and D). A similarly dramatic shift in the distribution of lumen phenotypes occurred at 250 µM RGD density. Nearly all (>90%) cysts in hydrogels presenting high densities of RGD peptide contained lumens, whereas the majority of cysts in low-density RGD gels lacked lumens (Fig. 4, C and E). The extent of cyst polarization and lumen formation was not different between PEG-4MAL hydrogels presenting 2,000 µM RGD peptide and collagen gels. These results show that although RGD peptide is not required for initial proliferation and generation of cell aggregates, differentiation of polarized cysts with lumens requires a threshold density of RGD in the matrix.

To explore the role of integrins in the RGD density–dependent effects on cyst phenotype within the synthetic hydrogel system, we cultured MDCK cells in PEG-4MAL hydrogels presenting 2,000 µM RGD peptide in the presence of LM609, an antibody that blocks binding of the αVβ3 integrin to RGD peptides, or AIIB2, an antibody that blocks the function of the β1 integrin that binds and assembles secreted laminin during cyst morphogenesis (Yu et al., 2005). Nearly all (>98%) cysts that developed in the presence AIIB2 or control isotype antibodies had normal, interior apical polarity (Fig. 4, F–H). In contrast, only 80% of epithelial cysts grown in the presence of LM609 exhibited interior apical polarity. Similarly, ~18% of cysts grown with AIIB2 or control antibodies exhibited a well-developed single lumen, whereas none of the cysts grown

in the presence of LM609 had well-formed, single lumens. These results demonstrate that the RGD-dependent effects on epithelial morphogenesis within PEG-4MAL are mediated by the αVβ3 integrin. Although statistically significant, the cyst phenotype shifts observed in RGD-presenting PEG-4MAL hydrogels in the presence of LM609 were considerably less than those seen in the absence of RGD. We attribute this discrepancy to the presence of other integrin heterodimers that bind RGD and provide significant signaling in the presence of LM609 (Teräväinen et al., 2013). The absence of a cyst phenotype shift in the presence of AIIB2 suggests that β1 integrin function is dispensable for polarized cyst morphogenesis in the RGD-functionalized synthetic hydrogel.

To demonstrate the versatility of the synthetic platform to study different adhesive ligands, we performed additional experiments for apicobasal polarization and lumen formation with other cysteine-terminated cell-adhesive peptides: laminin α1 chain–derived AG73 peptide (CGGRKRLQVQLSIRT; Hoffman et al., 1998), EF1zz peptide (CGGATLQLQEGRLHFXFD LGKGR, X: Nle; Suzuki et al., 2003), and collagen IV–derived peptide (CGGGEFYFDLRLKGDKY; Miles et al., 1994). This study showed peptide-specific differences in epithelial morphogenesis for MDCK cells (Fig. S5, A and B). We note that synthetic hydrogels presenting full-length proteins such as laminin and collagen can be prepared by blending the matrix protein with the PEG components during cross-linking, and these hydrogels also support lumen formation and polarization (Fig. S5 C). However, this approach has limitations, as these full-length proteins are considerable larger than the PEG macromer and will disrupt the local structure and cross-linking of the hydrogel, potentially resulting in ill-defined local mechanical and biochemical properties. At high concentrations of protein, these effects may be large enough such that performing dose-dependent studies as shown here for RGD peptide will be difficult.

A threshold level of ECM protease degradability is required for apicobasal polarity and lumen formation without alterations in cyst size

Epithelial morphogenesis requires local, cell-mediated matrix degradation to create space for expansion of cellular aggregates or extension of cellular processes (Weaver et al., 2014). We used two different experimental approaches to examine the effects of cross-link degradation on epithelial cyst development in PEG-4MAL hydrogels. First, we directly tuned the degradability of the hydrogel matrix by titrating a slower-degrading variant peptide (GPQ-A; Patterson and Hubbell, 2010) of the GPQ-W cross-linker in hydrogel formulations (4% polymer density, 2,000 µM RGD) that typically support high proliferation and formation of cell aggregates. Whereas 5% and 10% substitution of GPQ-A had no effect on cyst morphogenesis, GPQ-A content of 20% increased the incidence of abnormal polarity and altered lumen phenotypes (Fig. 5, A–C). GPQ-A content of >20% resulted in complete abrogation of cell proliferation and multicellular cyst precursor formation (Fig. 5 A). This result is consistent with the observation that cells did not proliferate or form cysts in PEG-4MAL gels of ≥5.0% polymer density with GPQ-W (Fig. 2).

We also incubated MDCK cells embedded in 4.0% PEG-4MAL hydrogels functionalized with RGD (2,000 µM) and cross-linked with GPQ-W in the broad-range matrix metalloproteinase (MMP) inhibitors GM6001 and MMPII. Interestingly,
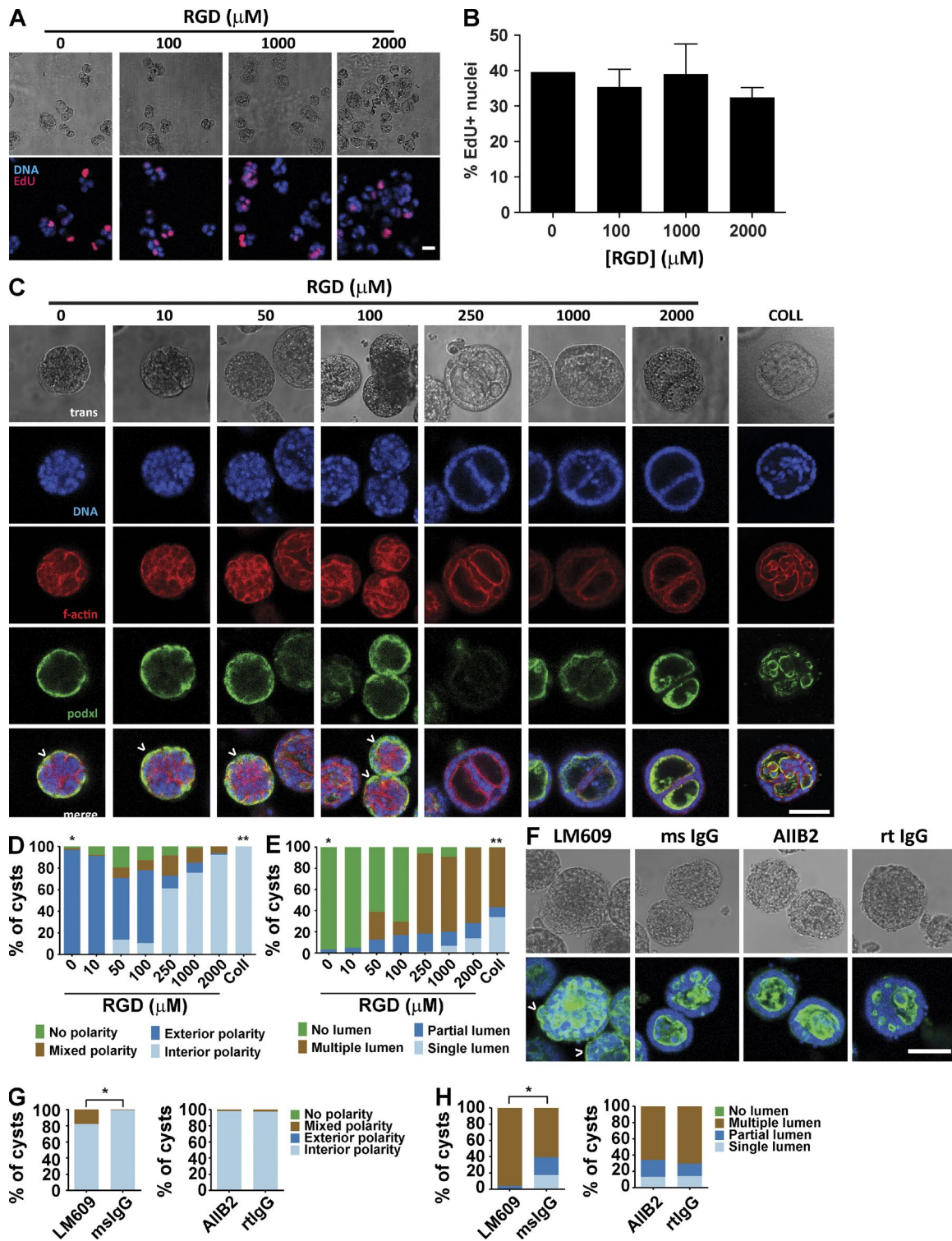
Figure 4. **Adhesive ligand density in PEG-4MAL hydrogel modulates cyst phenotype and apical polarity.** (A) Transmitted light and fluorescence microscopy images for MDCK cells cultured for 2 d in 4.0% PEG-4MAL hydrogels incorporating different amounts of RGD. Newly synthesized DNA was labeled by EdU. Bar, 20 µm. (B) Cell proliferation (mean ± SEM) at day 2 as assessed by EdU incorporation (>374 nuclei counted per condition). (C) Transmitted light and fluorescence microscopy images for MDCK cells cultured in 4.0% PEG-4MAL for 10 d and labeled for apical polarity marker gp135/podocalyxin (podxl). Inverted apical polarity indicated by ^. Bar, 50 µm. F-actin, filamentous actin. (D) Distribution of apical polarity phenotypes at day 10 (>78 cysts counted per condition). χ^2 test with Bonferroni's correction; *, P < 0.0001, 0 µM RGD versus every other condition except 10 µM RGD; **, P < 0.0001, collagen versus every other condition except 2,000 µM RGD. (E) Distribution of lumen phenotypes at day 10 (>78 cysts counted per condition). χ^2 test with Bonferroni's correction; *, P < 0.0001, 0 µM RGD versus every other condition except 10 µM RGD; **, P < 0.0001, collagen versus every other group. (F) MDCK cultured for 10 d in 4.0% PEG-4MAL gels with 2,000 µM RGD in the presence of function-blocking antibodies against integrin αVβ3 (LM609) or integrin β1 (AIIB2) or isotype control antibodies (mouse [ms] or rat [rt] IgG). Cysts were labeled with antibodies against gp135/podocalyxin (podxl). Bar, 50 µm. (G) Distribution of lumen phenotypes in F at day 10 (>100 cysts counted per condition). χ^2 test; *, P < 0.0001, mouse IgG versus LM609. (H) Distribution of apical polarity phenotypes in F at day 10 (>100 cysts counted per condition). χ^2 test; *, P < 0.0001, mouse IgG versus LM609.
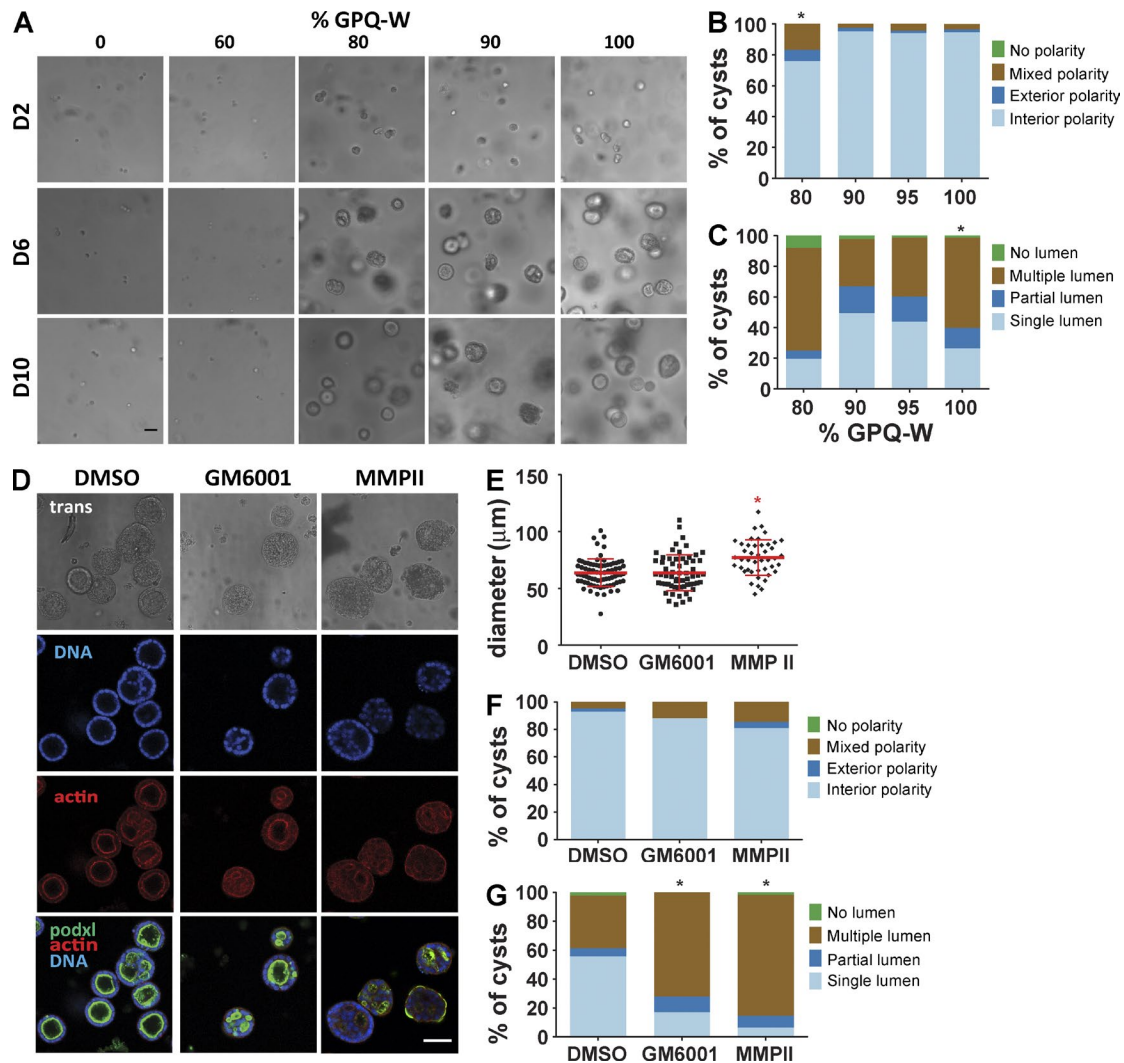
Figure 5. **Hydrogel cross-link degradation rate regulates cyst growth, lumen formation, and polarity.** (A) Transmitted light microscope images of MDCK cells cultures for 10 d in 4.0% PEG-4MAL hydrogels with 2,000 µM RGD cross-linked with either fast-degrading (GPQ-W) or slow-degrading (GPQ-A) cross-linking peptides titrated from 0% GPQ-W (100% GPQ-A) to 100% GPQ-W (0% GPQ-A). Bar, 50 µm. (B) Distribution of apical polarity phenotypes at day 10 (>135 cysts counted per condition). χ^2 test with Bonferroni's correction; *, $P < 0.0001$, 80% GPQ-W versus 100% GPQ-W. (C) Distribution of lumen phenotypes at day 10 (>135 cysts counted per condition). χ^2 test with Bonferroni's correction; *, $P < 0.005$, 100% GPQ-W versus all other conditions. (D) MDCK cells cultured for 10 d in PEG-4MAL hydrogels with 2,000 µM RGD and incubated with MMP inhibitors MMPII or GM6001 or control. Cysts were labeled with rhodamine phalloidin (filamentous actin), Hoechst 3342 (DNA), and an antibody against apical polarity marker gp135/podocalyxin (podxl; green). Bar, 50 µm. (E) Cyst size at day 10 (>44 cysts counted per condition). χ^2 test with Bonferroni's correction; *, $P < 0.05$, MMPII versus all other conditions. (F) Distribution of apical polarity phenotypes at day 10 (>108 cysts counted per condition). (G) Distribution of lumen phenotypes at day 10 (>108 cysts counted per condition). χ^2 test with Bonferroni's correction; *, $P < 0.0001$, GM6001 versus DMSO and MMPII versus DMSO.

these MMP inhibitors had modest effects on cyst size at day 10 (Fig. 5, D and E). However, both MMP inhibitors reduced the proportion of cysts with internal apical polarity and well-defined single lumen compared with the vehicle-only (DMSO) control (Fig. 5, D, F, and G). These alterations in cyst polarization and lumen formation mirror the effects of incorporating 20% of the slower-degrading GPQ-A cross-linking peptide in the permissive hydrogel formulation (Fig. 5 B). Taken together, these results show that MMP-dependent degradation of the PEG-4MAL hydrogel network is essential for normal epithelial morphogenesis within these synthetic ECM.

Synthetic ECM platform is applicable to study other epithelial cell models

We performed additional experiments with Caco-2 colon epithelial cells to demonstrate that the synthetic ECM platform

can be used to study epithelial morphogenesis with other cell systems. This study demonstrated that specific hydrogel formulations supported multicellular cyst assembly, lumen formation, and polarization with this epithelial cell line (Fig. 6). Interestingly, for Caco-2 cells, RGD adhesive peptide was required for multicellular cyst formation, as scrambled RDG-presenting gels supported poorly organized cell clusters with fewer cells. In addition, the range of permissive formulations for cyst formation occurred at higher polymer densities (6.0–8.0%) for Caco-2 cells compared with MDCK cells. Even though the hydrogel of 8.0% polymer density supported lumen formation and polarization, the resulting cysts were smaller than those developed in the formulation with 6.0% polymer density. These results show differences on the effects of ECM biochemical and biophysical cues on the morphogenetic program for different epithelial cell lines.
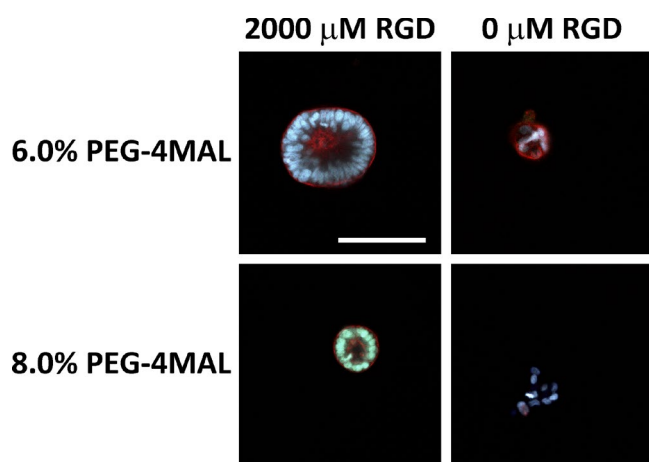
2000 μM RGD   **0 μM RGD**

6.0% PEG-4MAL

8.0% PEG-4MAL

Figure 6. **Hydrogel polymer density and RGD adhesive ligand regulate epithelial morphogenesis in Caco-2 cells.** Fluorescence microscopy images of Caco-2 cells grown within PEG-4MAL hydrogels for 10 d. Bar, 100 μm. Cysts were labeled with rhodamine phalloidin (filamentous actin) and Hoechst 3342 (DNA). Cyst formation, lumen formation, and polarization required RGD adhesive peptide. Hydrogel polymer density influences the size of the resulting epithelial cyst.

Discussion

This study establishes a modular synthetic ECM-mimetic hydrogel platform with controlled presentation of cell-adhesive ligands, tunable mechanical properties, and protease-dependent degradation that can be precisely engineered to study the contributions of ECM biophysical and biochemical properties on the epithelial morphogenetic program. Systematic changes in hydrogel formulation to independently tune hydrogel polymer density, elasticity, adhesive ligand density, and protease-dependent degradation revealed that each of these properties has profound effects on specific stages of this coordinated morphogenetic process, including proliferation, multicellular cyst development, polarization, and lumen formation. Importantly, these effects occur via mechanisms that parallel development in natural matrices. Because of their inherent complexity, these new insights into the contributions of ECM biochemical and mechanical properties to the regulation of epithelial morphogenesis are simply not tractable using natural collagen and laminin ECMs. Remarkably, a spectrum of developmental outcomes including cell apoptosis, normal cyst development comprising a spherical polarized cell monolayer enclosing a single lumen, and abnormal cellular assemblies consisting of solid spheres with no lumen or structures with inverted polarity and multiple lumens reminiscent of pathological states could be engineered within the same synthetic hydrogel platform.

We identified synthetic hydrogel formulations that supported the epithelial morphogenesis program to the same extent as type I collagen matrices. Interestingly, the collagen gels used as a reference in the experiments presented here have a fibrillar architecture with micrometer-sized pores, whereas the PEG-4MAL gels have an amorphous structure with a nanoscale mesh size. Our results suggest that the epithelial morphogenesis program is insensitive to these differences in matrix architecture. However, because of the complex nature of the collagen gels, it is difficult to determine whether other important parameters (e.g., adhesive ligand density) regulating epithelial

morphogenesis are equivalent between the optimal synthetic analog and the natural ECM.

Our results for the effects of ECM properties on the normal epithelial morphogenetic program are fundamentally different from those reported for cancer cells in synthetic gels, most likely reflecting central differences between developmental morphogenesis and tumorigenesis. For instance, MDCK cell proliferation and assembly into multicellular structures was insensitive to RGD peptide density, whereas cyst polarity and lumen phenotypes showed a dramatic dependence on RGD density. Additionally, the literature has major inconsistencies regarding the effects of polymer density (equated in these papers to stiffness) on the organization of cancer cells into aggregates of varying size (Gill et al., 2012; Beck et al., 2013; Raza et al., 2013). We observe different responses for normal epithelial cells. Multicellular cysts formed at polymer densities below a threshold that supported cell proliferation; above this threshold, no cell aggregates were formed owing to inhibited proliferation and apoptosis. Moreover, for permissive formulations, we report polymer density-dependent differences in the establishment of apicobasal polarity and the formation of cysts with no lumen, a single lumen, and multiple lumens, which are hallmarks of normal epithelial morphogenesis and formation of a rudimentary epithelial organ. Yet all these cysts had equivalent size. Raza et al. reported that hydrogels that were not protease-degradable did not support formation of larger cell aggregates (Raza et al., 2013). This result is the expected consequence of a tight hydrogel network encapsulating the cells. In the present study, we show this effect for a hydrogel with 100% nondegradable cross-links. However, we also find that intermediate levels of protease-degradability regulate apicobasal polarity and lumen phenotypes without alterations in cyst size, demonstrating that protease-degradability of the ECM regulates these critical epithelial characteristics independently of simply constraining cells from forming cell aggregates.

We expect that this biomaterial platform will find widespread adoption in developmental cell and tumor biology fields to study ECM-regulated morphogenetic processes. Furthermore, this technology enables the engineering of instructive epithelial synthetic niches for cell expansion and controlled differentiation as well as delivery vehicles for regenerative medicine applications that overcome the limitations of natural matrices such as lot-to-lot variability and regulatory and translational constraints.

Materials and methods

Antibodies and labeling reagents

Primary antibodies used were mouse anti-gp135/podocalyxin (clone 3F21D8; provided by G. Ojakian, SUNY Downstate Medical Center, Brooklyn, NY), rabbit anti-laminin (Sigma-Aldrich), mouse anti-αvβ3 integrin (LM609; EMD Millipore), rat anti–β1 integrin (AIIB2; Developmental Studies Hybridoma Bank), mouse anti-GM130 (BD Transduction Laboratories), mouse anti-ZO-1 (Life Technologies), and rabbit anti–β-catenin (H-102; Santa Cruz Biotechnology). The following secondary antibodies were used: goat anti–mouse IgG Alexa Fluor 488, goat anti–rat IgG Alexa Fluor 555, goat anti–rabbit IgG Alexa Fluor 488 (Life Technologies), and donkey anti–rabbit IgG Dylight649 (Thermo Fisher Scientific). Nuclei were stained with Hoechst 33342, and filamentous actin was stained with rhodamine phalloidin (Life Technologies).

Cell culture and hydrogel formation

MDCK strain II epithelial cells (Sigma-Aldrich) were maintained in Eagle's minimal essential media (EMEM; ATCC) supplemented with fetal bovine serum (Life Technologies) at 10% (vol/vol), penicillin (100 IU/ml) and streptomycin (100 µg/ml), and fungizone.

To prepare PEG hydrogels, PEG-4MAL (MW 22,000; Laysan Bio) was dissolved in a triethanolamine (TEA) buffer (4 mM in DPBS, pH 7.4). Adhesive and cross-linking peptides were custom-synthesized by AAPPTec. Adhesive peptide (GRGDSPC) or nonadhesive peptide (GRDGSPC) or combination was dissolved in TEA to generate functionalized PEG-4MAL precursor. Bis-cysteine cross-linking peptide GCRDGPQG↓IWGQDRCG (GPQ-W; ↓ denotes enzymatic cleavage site) or GCRDGPQG↓IAGQDRCG (GPQ-A) was dissolved in TEA at 1:1 maleimide/cysteine ratio after accounting for maleimide groups reacted with adhesive peptide. MDCK cells were resuspended at 5× final cell density in ice-cold serum-free EMEM and kept on ice. To form gels, adhesive peptide-functionalized PEG-4MAL macromer, cells, and cross-linking peptides were polymerized under serum-free conditions for 20 min before addition of complete medium. For studies with integrin-blocking antibodies, cells were preincubated (30 min, gentle rocking, at 22°C) in 0.1% bovine serum albumin in serum-free EMEM containing antibodies. For collagen gels, type I collagen from bovine tendon (3 mg/ml; Sigma-Aldrich) was mixed with cell suspension in serum-free media to achieve a 2.0 mg/ml type I collagen gels cast onto polyester permeable supports (0.4-µm pore; Corning) in a 24-well plate.

Hydrogel characterization

Hydrogel elastic modulus measurements were obtained by atomic force microscopy as described previously (Phelps et al., 2012) with cantilever spring constants of 10 mN/m, indentation speed of ~2.0 µm/s, and force trigger set point of 1.25 nN. Using an MFP-3D-BIO atomic force microscope (Asylum Research), samples were probed under fluid conditions (ultrapure H_2O) using a pyramidal-tipped silicon nitride cantilever (Bruker). The force–indentation curve was obtained for each measurement and then analyzed with a Hertzian model for a pyramidal tip (Wavemetrics; IgorPro software routines), from which the Young's modulus values were calculated. The sample Poisson's ratio was assumed as 0.33, and a power law of 2.0 for the sample indentation distance was used to model tip geometry. Hydrogel mass swelling ratio and ligand tethering were measured as described previously (Phelps et al., 2012). The storage and loss moduli of hydrogels were assessed by dynamic oscillatory strain and frequency sweeps performed on a MCR 302 stress-controlled rheometer (Anton Paar) with a 9-mm diameter, 2° cone, and plate geometry. Oscillatory frequency sweeps were used to examine the storage and loss moduli ($\omega = 0.5$–100 rad s^{-1}) at a strain of 1%. For permeability experiments, hydrogels were incubated in FITC-labeled α-bungarotoxin (500 µg/ml), and signal intensity at the center of the gel sample was measured over time via confocal microscopy. Intensity profiles were fit to Fick's second law to obtain diffusion coefficients (Koutsopoulos et al., 2009). For ligand mobility studies, a Ti-E inverted microscope (Nikon) with Perfect Focus System and C2-Plus Confocal System with a Plan Fluor 40× (NA 0.75) objective was used for FRAP. Hydrogels were prepared with Alexa Fluor 594–labeled RGD peptide and allowed to equilibrate. Initial fluorescence intensity was measured using low laser power followed by photobleaching of a 0.20-mm-diameter circle within the hydrogel at 38 mW with 561-nm laser for 10 s. The recovery of fluorescence was monitored for up to 5.8 h. Image series were imported into MATLAB, where background subtraction and correction for incidental bleaching during image acquisition were applied to data extracted from the bleached region. For analysis of cell-dependent RGD peptide clustering, MDCK cells were cultured within hydrogels presenting a mixture of Alexa Fluor 594–labeled and control RGD peptide for 8 d. Fluorescence signal intensity was measured for 35 min at different radial positions from the cell–hydrogel interface in the presence or absence of 10 µM Y-27632.

RGD labeling

RGD peptide was labeled using Alexa Fluor 594 NHS-ester dye (Life Technologies). To quantify labeling efficiency, size-exclusion chromatography was performed using a HiPrep Sephacryl S-100 HR gel filtration column on an AKTA Pure 25 chromatography system (GE Healthcare). DPBS supplemented with 0.15 M NaCl was used as the elution buffer to separate conjugated from unconjugated dye at a volumetric rate of 0.5 ml/min. Onboard absorbance readings of the eluted sample at 280/594 nm yielded a set of curves with peaks that corresponded to labeled and unlabeled peptide. Quantification of the area under the peaks was determined, and the ratio of the areas was used as the labeling efficiency.

Viability and proliferation assays

PEG-4MAL gels were incubated in 0.5% collagenase I (Worthington Biochemical), 2 µM calcein-AM (live), and 1 µM TOTO-3 iodide (dead; Life Technologies) in serum-free EMEM media until hydrogel was completely dissolved and cells settled at bottom of well. For collagen gels, gel was incubated in 2 µM calcein-AM and 1 µM TOTO-3 for 30 min and placed in chambered coverglass for imaging. Proliferation was assayed using the Click-iT EdU Imaging Kit (Life Technologies). Samples were imaged with Nikon Plan Fluor 10× (NA 0.30) or Plan Fluor 20× (NA 0.45) objectives in a Nikon Eclipse TE2000 inverted microscope and C1 Confocal System (EZ-C1 acquisition software) or Ti-E inverted microscope with Perfect Focus System and C2-Plus Confocal System (NIS Elements acquisition software). Cells were counted with ImageJ macros.

Immunofluorescence labeling of cysts

Gels were washed extensively in DPBS and fixed in 4% formaldehyde in DPBS for 15 min. Gels were incubated for 30 min in blocking buffer (1% bovine serum albumin, 1% goat serum, 0.1% fish skin gelatin, 0.5% Triton X-100, and 0.05% sodium azide in PBS). Samples were incubated in primary antibodies diluted in blocking buffer on an orbital shaker at 4°C overnight. Secondary antibodies and nuclear stain were diluted in blocking buffer and incubated on an orbital shaker at 4°C overnight. After immunostaining, cysts were recovered by collagenase digestion and mounted in 2% low-melt agarose. Fluorescent images for cyst scoring were captured with Nikon Plan Fluor 20× (NA 0.45) or Plan Apo 60× (NA 1.40) objectives in a Nikon Eclipse TE2000 inverted microscope and C1 Confocal System (EZ-C1 acquisition software) or Ti-E inverted microscope with Perfect Focus System and C2-Plus Confocal System (NIS Elements acquisition software). Cyst size was measured from fluorescent images of cyst cross sections using ImageJ FIJI package. The following scoring system was used for polarity: (1) interior apical polarity: a cyst cross section in which the interior of one or more lumens is lined with gp135 staining and the exterior of cyst lacks gp135 staining; (2) exterior apical polarity: a cyst cross section in which the interior of one or more lumens lacks gp135 staining and the exterior of cyst is lined with gp135 staining; (3) mixed apical polarity: a cyst cross section in which the interior of one or more lumens and the exterior of cysts show staining for gp135; and (4) no apical polarity: a cyst cross section with no staining for gp135. The following scoring system was used for lumen phenotypes: (1) single lumen: a cyst cross section having a single hollow space and outlined by a monolayer of cells; (2) partial lumen: a cyst cross section having a single hollow space bounded by multiple layers or groups of cells; (3) multiple lumens: a cyst cross section having multiple hollow spaces; and (4) no lumen: a cyst cross section having no hollow spaces. Fig. S3 presents exemplary cysts for each scoring category.

Statistical analyses

Results are presented either as mean ± SEM or percentages of population. Statistical analyses were performed using GraphPad Prism 6.0. For normally distributed data with equal variances, one-way analysis of variance with Tukey's multiple comparison test was used. For categorical data such as polarity and lumen phenotypes, χ^2 test with Bonferroni's test for multiple comparisons was used. A p-value <0.05 was considered significant.

Online supplemental material

Fig. S1 shows adhesive ligand mobility within PEG hydrogels. Fig. S2 shows epithelial cyst polarization and lumen formation. Fig. S3 shows that epithelial cysts within PEG-4MAL hydrogels exhibit canonical markers of apicobasal polarity and lumen phenotypes. Fig. S4 shows biophysical characterization and epithelial cyst phenotypes for PEG-4MAL hydrogel formulations generated with different macromer sizes. Fig. S5 shows epithelial cyst phenotypes for PEG-4MAL hydrogels presenting different adhesive peptides. Online supplemental material is available at http://www.jcb.org/cgi/content/full/jcb.201506055/DC1. Additional data are available in the JCB DataViewer at http://dx.doi .org/10.1083/jcb.201506055.dv.

References

Barcellos-Hoff, M.H., J. Aggeler, T.G. Ram, and M.J. Bissell. 1989. Functional differentiation and alveolar morphogenesis of primary mammary cultures on reconstituted basement membrane. *Development.* 105:223–235.

Beck, J.N., A. Singh, A.R. Rothenberg, J.H. Elisseeff, and A.J. Ewald. 2013. The independent roles of mechanical, structural and adhesion characteristics of 3D hydrogels on the regulation of cancer invasion and dissemination. *Biomaterials.* 34:9486–9495. http://dx.doi.org/10.1016/j.biomaterials.2013.08.077

Bryant, D.M., and K.E. Mostov. 2008. From cells to organs: building polarized tissue. *Nat. Rev. Mol. Cell Biol.* 9:887–901. http://dx.doi.org/10.1038/nrm2523

Canal, T., and N.A. Peppas. 1989. Correlation between mesh size and equilibrium degree of swelling of polymeric networks. *J. Biomed. Mater. Res.* 23:1183–1193. http://dx.doi.org/10.1002/jbm.820231007

Flory, P.J., and J. Rehner. 1943. Statistical mechanics of cross-linked polymer networks II. Swelling. *J. Chem. Phys.* 11:1183–1193.

Ghajar, C.M., X. Chen, J.W. Harris, V. Suresh, C.C. Hughes, N.L. Jeon, A.J. Putnam, and S.C. George. 2008. The effect of matrix density on the regulation of 3-D capillary morphogenesis. *Biophys. J.* 94:1930–1941. http://dx.doi.org/10.1529/biophysj.107.120774

Gill, B.J., D.L. Gibbons, L.C. Roudsari, J.E. Saik, Z.H. Rizvi, J.D. Roybal, J.M. Kurie, and J.L. West. 2012. A synthetic matrix with independently tunable biochemistry and mechanical properties to study epithelial morphogenesis and EMT in a lung adenocarcinoma model. *Cancer Res.* 72:6013–6023. http://dx.doi.org/10.1158/0008-5472.CAN-12-0895

Hoffman, M.P., M. Nomizu, E. Roque, S. Lee, D.W. Jung, Y. Yamada, and H.K. Kleinman. 1998. Laminin-1 and laminin-2 G-domain synthetic peptides bind syndecan-1 and are involved in acinar formation of a human submandibular gland cell line. *J. Biol. Chem.* 273:28633–28641. http://dx.doi.org/10.1074/jbc.273.44.28633

Huebsch, N., P.R. Arany, A.S. Mao, D. Shvartsman, O.A. Ali, S.A. Bencherif, J. Rivera-Feliciano, and D.J. Mooney. 2010. Harnessing traction-mediated manipulation of the cell/matrix interface to control stem-cell fate. *Nat. Mater.* 9:518–526. http://dx.doi.org/10.1038/nmat2732

Hughes, C.S., L.M. Postovit, and G.A. Lajoie. 2010. Matrigel: a complex protein mixture required for optimal growth of cell culture. *Proteomics.* 10:1886–1890. http://dx.doi.org/10.1002/pmic.200900758

Khetan, S., M. Guvendiren, W.R. Legant, D.M. Cohen, C.S. Chen, and J.A. Burdick. 2013. Degradation-mediated cellular traction directs stem cell fate in covalently crosslinked three-dimensional hydrogels. *Nat. Mater.* 12:458–465. http://dx.doi.org/10.1038/nmat3586

Klinowska, T.C., J.V. Soriano, G.M. Edwards, J.M. Oliver, A.J. Valentijn, R. Montesano, and C.H. Streuli. 1999. Laminin and beta1 integrins are crucial for normal mammary gland development in the mouse. *Dev. Biol.* 215:13–32. http://dx.doi.org/10.1006/dbio.1999.9435

Kloxin, A.M., A.M. Kasko, C.N. Salinas, and K.S. Anseth. 2009. Photodegradable hydrogels for dynamic tuning of physical and chemical properties. *Science.* 324:59–63. http://dx.doi.org/10.1126/science.1169494

Koutsopoulos, S., L.D. Unsworth, Y. Nagai, and S. Zhang. 2009. Controlled release of functional proteins through designer self-assembling peptide nanofiber hydrogel scaffold. *Proc. Natl. Acad. Sci. USA.* 106:4623–4628. http://dx.doi.org/10.1073/pnas.0807506106

Leventa, K.R., H. Yu, L. Kass, J.N. Lakins, M. Egeblad, J.T. Erler, S.F. Fong, K. Csiszar, A. Giaccia, W. Weninger, et al. 2009. Matrix crosslinking forces tumor progression by enhancing integrin signaling. *Cell.* 139:891–906. http://dx.doi.org/10.1016/j.cell.2009.10.027

Lubarsky, B., and M.A. Krasnow. 2003. Tube morphogenesis: making and shaping biological tubes. *Cell.* 112:19–28. http://dx.doi.org/10.1016/S0092-8674(02)01283-7

Lutolf, M.P., G.P. Raeber, A.H. Zisch, N. Tirelli, and J.A. Hubbell. 2003. Cell-responsive synthetic hydrogels. *Adv. Mater.* 15:888–892. http://dx.doi.org/10.1002/adma.200304621

Martín-Belmonte, F., W. Yu, A.E. Rodríguez-Fraticelli, A.J. Ewald, Z. Werb, M.A. Alonso, and K. Mostov. 2008. Cell-polarity dynamics controls the mechanism of lumen formation in epithelial morphogenesis. *Curr. Biol.* 18:507–513. http://dx.doi.org/10.1016/j.cub.2008.02.076

McAteer, J.A., A.P. Evan, E.E. Vance, and K.D. Gardner. 1986. MDCK cysts: An in vitro model of epithelial cyst formation and growth. *Methods Cell Sci.* 10:245–248.

Miles, A.J., A.P. Skubitz, L.T. Furcht, and G.B. Fields. 1994. Promotion of cell adhesion by single-stranded and triple-helical peptide models of basement membrane collagen alpha 1(IV)531-543. Evidence for conformationally dependent and conformationally independent type IV collagen cell adhesion sites. *J. Biol. Chem.* 269:30939–30945.

Mroue, R., and M.J. Bissell. 2013. Three-dimensional cultures of mouse mammary epithelial cells. *Methods Mol. Biol.* 945:221–250. http://dx.doi .org/10.1007/978-1-62703-125-7_14

Nelson, C.M., M.M. Vanduijn, J.L. Inman, D.A. Fletcher, and M.J. Bissell. 2006. Tissue geometry determines sites of mammary branching morphogenesis in organotypic cultures. *Science.* 314:298–300. http://dx.doi.org/10.1126/science.1131000

O'Brien, L.E., T.S. Jou, A.L. Pollack, Q. Zhang, S.H. Hansen, P. Yurchenco, and K.E. Mostov. 2001. Rac1 orientates epithelial apical polarity through effects on basolateral laminin assembly. *Nat. Cell Biol.* 3:831–838. http://dx.doi.org/10.1038/ncb0901-831

O'Brien, L.E., M.M. Zegers, and K.E. Mostov. 2002. Opinion: Building epithelial architecture: insights from three-dimensional culture models. *Nat. Rev. Mol. Cell Biol.* 3:531–537. http://dx.doi.org/10.1038/nrm859

O'Brien, L.E., W. Yu, K. Tang, T.S. Jou, M.M. Zegers, and K.E. Mostov. 2006. Morphological and biochemical analysis of Rac1 in three-dimensional epithelial cell cultures. *Methods Enzymol.* 406:676–691. http://dx.doi.org/10.1016/S0076-6879(06)06053-8

Paszek, M.J., N. Zahir, K.R. Johnson, J.N. Lakins, G.I. Rozenberg, A. Gefen, C.A. Reinhart-King, S.S. Margulies, M. Dembo, D. Boettiger, et al. 2005. Tensional homeostasis and the malignant phenotype. *Cancer Cell.* 8:241–254. http://dx.doi.org/10.1016/j.ccr.2005.08.010

Patterson, J., and J.A. Hubbell. 2010. Enhanced proteolytic degradation of molecularly engineered PEG hydrogels in response to MMP-1 and MMP-2. *Biomaterials.* 31:7836–7845. http://dx.doi.org/10.1016/j.biomaterials .2010.06.061

Phelps, E.A., N.O. Enemchukwu, V.F. Fiore, J.C. Sy, N. Murthy, T.A. Sulchek, T.H. Barker, and A.J. García. 2012. Maleimide cross-linked bioactive PEG hydrogel exhibits improved reaction kinetics and cross-linking for cell encapsulation and in situ delivery. *Adv. Mater.* 24:64–70: 2. http://dx .doi.org/10.1002/adma.201103574

Phelps, E.A., D.M. Headen, W.R. Taylor, P.M. Thulé, and A.J. García. 2013. Vasculogenic bio-synthetic hydrogel for enhancement of pancreatic islet engraftment and function in type 1 diabetes. *Biomaterials.* 34:4602–4611. http://dx.doi.org/10.1016/j.biomaterials.2013.03.012

Provenzano, P.P., D.R. Inman, K.W. Eliceiri, and P.J. Keely. 2009. Matrix density-induced mechanoregulation of breast cell phenotype, signaling and gene expression through a FAK-ERK linkage. *Oncogene.* 28:4326–4343. http://dx.doi.org/10.1038/onc.2009.299

Raza, A., C.S. Ki, and C.C. Lin. 2013. The influence of matrix properties on growth and morphogenesis of human pancreatic ductal epithelial cells in 3D. *Biomaterials.* 34:5117–5127. http://dx.doi.org/10.1016/j .biomaterials.2013.03.086

Roignot, J., X. Peng, and K. Mostov. 2013. Polarity in mammalian epithelial morphogenesis. *Cold Spring Harb. Perspect. Biol.* 5:a013789. http://dx .doi.org/10.1101/cshperspect.a013789

Salimath, A.S., E.A. Phelps, A.V. Boopathy, P.L. Che, M. Brown, A.J. García, and M.E. Davis. 2012. Dual delivery of hepatocyte and vascular endothelial growth factors via a protease-degradable hydrogel improves cardiac function in rats. *PLoS One.* 7:e50980. http://dx.doi.org/10.1371/ journal.pone.0050980

Suzuki, N., H. Nakatsuka, M. Mochizuki, N. Nishi, Y. Kadoya, A. Utani, S. Oishi, N. Fujii, H.K. Kleinman, and M. Nomizu. 2003. Biological activities of homologous loop regions in the laminin alpha chain G domains. *J. Biol. Chem.* 278:45697–45705. http://dx.doi.org/10.1074 /jbc.M304667200

Teräväinen, T.P., S.M. Myllymäki, J. Friedrichs, N. Strohmeyer, J.V. Moyano, C. Wu, K.S. Matlin, D.J. Muller, and A. Manninen. 2013. αV-integrins are required for mechanotransduction in MDCK epithelial cells. *PLoS One.* 8:e71485. http://dx.doi.org/10.1371/journal.pone.0071485

Weaver, S.A., B. Wolters, N. Ito, A.M. Woskowicz, K. Kaneko, Y. Shitomi, M. Seiki, and Y. Itoh. 2014. Basal localization of MT1-MMP is essential for epithelial cell morphogenesis in 3D collagen matrix. *J. Cell Sci.* 127:1203–1213. http://dx.doi.org/10.1242/jcs.135236

Weiss, M.S., B.P. Bernabé, A. Shikanov, D.A. Bluver, M.D. Mui, S. Shin, L.J. Broadbelt, and L.D. Shea. 2012. The impact of adhesion peptides within hydrogels on the phenotype and signaling of normal and cancerous mammary epithelial cells. *Biomaterials.* 33:3548–3559. http://dx.doi.org /10.1016/j.biomaterials.2012.01.055

Wozniak, M.A., R. Desai, P.A. Solski, C.J. Der, and P.J. Keely. 2003. ROCK-generated contractility regulates breast epithelial cell differentiation in response to the physical properties of a three-dimensional collagen matrix. *J. Cell Biol.* 163:583–595. http://dx.doi.org/10.1083/jcb.200305010

Yu, W., A. Datta, P. Leroy, L.E. O'Brien, G. Mak, T.S. Jou, K.S. Matlin, K.E. Mostov, and M.M. Zegers. 2005. Beta1-integrin orients epithelial polarity via Rac1 and laminin. *Mol. Biol. Cell.* 16:433–445. http://dx.doi .org/10.1091/mbc.E04-05-0435

Zhang, H., F. Landmann, H. Zahreddine, D. Rodriguez, M. Koch, and M. Labouesse. 2011. A tension-induced mechanotransduction pathway promotes epithelial morphogenesis. *Nature.* 471:99–103. http://dx.doi .org/10.1038/nature09765

Zhang, X., G. Mernaugh, D.H. Yang, L. Gewin, M.B. Srichai, R.C. Harris, J.M. Iturregui, R.D. Nelson, D.E. Kohan, D. Abrahamson, et al. 2009. beta1 integrin is necessary for ureteric bud branching morphogenesis and maintenance of collecting duct structural integrity. *Development.* 136:3357–3366. http://dx.doi.org/10.1242/dev.036269